

---

# Masked-RPCA: Sparse and Low-rank Decomposition Under Overlaying Model and Application to Moving Object Detection

---

Amirhossein Khalilian-Gourtani<sup>1</sup> Shervin Minaee<sup>2</sup> Yao Wang<sup>1</sup>

## Abstract

Foreground detection in a given video sequence is a pivotal step in many computer vision applications such as video surveillance system. Robust Principal Component Analysis (RPCA) performs low-rank and sparse decomposition and accomplishes such a task when the background is stationary and the foreground is dynamic and relatively small. A fundamental issue with RPCA is the assumption that the low-rank and sparse components are added at each element, whereas in reality, the moving foreground is overlaid on the background. We propose the representation via masked decomposition (i.e. an overlaying model) where each element either belongs to the low-rank or the sparse component, decided by a mask. We propose the Masked-RPCA algorithm to recover the mask and the low-rank components simultaneously, utilizing linearizing and alternating direction techniques. We further extend our formulation to be robust to dynamic changes in the background and enforce spatial connectivity in the foreground component. Our study shows significant improvement of the detected mask compared to post-processing on the sparse component obtained by other frameworks.

## 1. Introduction

Sparse and low-rank decomposition has been an active research area in signal and image processing in the past decade, with applications in motion segmentation (Cao et al., 2016), (Gao et al., 2014), image foreground extraction (Ebadi & Izquierdo, 2016), and optics (Kafieh et al., 2015). In the simplest case, this problem can be formulated as:

$$\underset{L,S}{\text{minimize}} \quad \text{rank}(L) + \lambda_s \|S\|_0 \quad \text{s.t.} \quad X = L + S, \quad (1)$$

<sup>1</sup>Electrical and Computer Engineering Department, New York University. <sup>2</sup>Expedia Inc.. Correspondence to: Amirhossein Khalilian-Gourtani <akg404@nyu.edu>.

Preliminary work. Submitted to the International Conference on Machine Learning (ICML).

where  $L$  and  $S$  denote the low-rank and sparse components of the signal  $X$ , respectively. There are some situations in which a unique decomposition may not exist; e.g. if the low-rank matrix  $L$  itself is also very sparse, it becomes very hard to uniquely identify it from another sparse matrix. Therefore, there have been many studies to find the conditions under which this decomposition is possible, such as the works in (Candès et al., 2011), (Feng et al., 2013). Also because of the non-convexity of both the rank function and the  $\ell_0$  norm, the problem in (1) is NP-hard. In order to be able to solve this decomposition, usually the  $\text{rank}(L)$  is relaxed to  $\|L\|_*$  (the nuclear norm of  $L$ , which is the sum of its singular values), and the  $\|S\|_0$  is relaxed by the  $\|S\|_1$  approximation (Recht et al., 2010).

The dominant application of sparse and low-rank decomposition (aka RPCA) has been for moving object detection in videos (Chen et al., 2012), (Zhang et al., 2013), but it has also been used for various other applications. To name some of the prominent works, in (Peng et al., 2012), Peng et al proposed a sparse and low-rank decomposition approach with application for robust image alignment. A similar approach has been proposed by Zhang (Zhang et al., 2012) for transform invariant low-rank textures. In (Keshavan et al., 2010), Keshavan proposed an algorithm for matrix completion using low-rank decomposition.

There has been several improvement of the vanilla RPCA over the past decade, and despite their great improvements in terms of accuracy and speed, there is a fundamental limitation in most of these models. The basic assumption that all these models share is the additive model for the sparse and low-rank components. In reality, the dynamic foreground object is overlaid on top of the low-rank background. For a more detailed overview of RPCA extensions, we refer the readers to (Yazdi & Bouwmans, 2018).

In this work, we try to address this issue by assuming a model for the case where the two components are overlaid on top of each other (instead of simply being added). Thus, each element of  $X$  comes only from one of the components. Therefore, besides deriving the sparse and low-rank component we need to find their supports. Assuming  $W \in \{0, 1\}^{mn \times k}$  denotes the support of  $S$ , we can write this overlaid signal summation as  $X = (1 - W) \circ L + W \circ S$ .

We can separate these components by assuming some prior knowledge on  $L$ ,  $S$  and  $W$  terms, and forming an optimization problem. In fact, we do not need to even include the  $S$  term in our optimization framework, since by having  $W$ , the  $S$  component can easily be derived as  $S = W \circ X$ . We propose an optimization algorithm (to be called M-RPCA) based on the alternating direction method of multipliers (ADMM) (Boyd et al., 2011) and ideas of linearizing (Lin et al., 2011). We show the convergence of the proposed algorithm to a Karush–Kuhn–Tucker (KKT) point under reasonable assumptions. Our experiments show that the proposed framework directly recovers the mask of the foreground without need for post processing on the sparse component as in the RPCA algorithm.

As with the original RPCA algorithm, the proposed M-RPCA algorithm has two limitations: 1) It does not enforce spatial connectivity of the foreground, and 2) when the background is not stationary and has random perturbations (such as water waves, moving leaves, etc.), these perturbations are usually picked up by the sparse component, leading to noisy foreground detection. We further show extensions of the proposed framework to tackle these problems. Following the idea of (Cao et al., 2016), we model the background as the sum of a low rank component and a sparse component (used to model the random perturbation in the dynamic background), and furthermore enforce the spatial connectivity of the foreground object by adding a total variation penalty on the mask in the optimization formulation. We propose an optimization algorithm (to be called extended M-RPCA or EM-RPCA) to solve for all three components and show that it leads to significant improvement over M-RPCA in sequences with dynamic background.

The idea of solving a masked decomposition problem was first proposed in (Minaee & Wang, 2017) for image segmentation, where an image is considered to have two overlaid components (e.g. text overlaid on background), each modeled by a subspace. Here, we extend this work by assuming one component is low-rank, while the other is sparse.

The structure of the rest of this paper is as follows: Section II presents the problem formulation, and the proposed optimization framework to solve it, as well as a convergence analysis. Section III provides the detailed experimental results of the proposed framework for moving object detection, and its comparison with previous state-of-the-arts models. And finally the paper is concluded in Section V.

## 2. Problem Formulation and Solution

In this section we introduce the general framework of masked robust principal component analysis (Masked-RPCA) formulated as an optimization problem, propose an algorithmic solution based on ADMM and linearizing

techniques, and investigate the convergence properties.

### 2.1. Masked Robust Principal Component Analysis

Given a sequence of video frames in  $X^{3d} \in \mathbb{R}^{m \times n \times k}$  let us denote the matrix  $X \in \mathbb{R}^{mn \times k}$  which is constructed by vectorizing and stacking the frames of the video. Then, the goal is to recover the matrices  $L \in \mathbb{R}^{mn \times k}$  and  $W \in \{0, 1\}^{mn \times k}$  such that  $W$  denotes the foreground support and the low-rank matrix  $L$  matches the video sequence  $X$  wherever the foreground is not active. A plausible formulation of such problem can be written as (2).

$$\begin{aligned} & \underset{L, W}{\text{minimize}} && \text{rank}(L) + \lambda_w \psi(W) \\ & \text{subject to:} && (1 - W) \circ (X - L) = 0 \\ & && W \in \{0, 1\}^{mn \times k} \end{aligned} \quad (2)$$

where  $\psi(\cdot)$  encodes our prior knowledge about  $W$  and  $\lambda_w \in \mathbb{R}$  is the regularization parameter. The problem as stated in (2) is not tractable because 1) the general rank minimization problem is NP-hard (Recht et al., 2010), and 2) recovering the binary matrix  $W$  requires solving a combinatorial problem. To manage the rank minimization in general, nuclear norm minimization is proposed as a surrogate especially in the context of matrix completion (Recht et al., 2010; Candès et al., 2011). Additionally, the  $W \in \{0, 1\}^{mn \times k}$  constraint can be relaxed to the convex interval between zero and one, namely,  $W \in [0, 1]^{mn \times k}$ . Imposing the sparsity of desired  $W$  via  $\ell_1$ -norm we can formulate the problem as in (3).

$$\begin{aligned} & \underset{L, W}{\text{minimize}} && \|L\|_* + \lambda_w \|W\|_1 \\ & \text{subject to:} && (1 - W) \circ (X - L) = 0 \\ & && W \in [0, 1]^{mn \times k} \end{aligned} \quad (3)$$

The algorithm for solving the problem in (3) is not immediately apparent especially since the variables  $W$  and  $L$  are coupled. For general low-rank and sparse decomposition formulations the ADMM algorithm is shown to be effective (Candès et al., 2011). More recently, ADMM for multi-affine constraints under certain assumptions was introduced and analyzed (Goldfarb, 2018). Additionally, ideas of linearizing such as Linearized Alternating Direction Method (LADM) for general affine constraint (Lin et al., 2011) and for nuclear norm minimization (Yang & Yuan, 2013) were introduced to handle more complicated affine constraints. Here, we propose to use the linearizing techniques for the bi-affine constraint as in (3). This way not only we can deal with the coupling of the variables but also we will find closed form solution for each sub-problem of the ADMM algorithm.

In the following section we drive the steps of the algorithm by forming the augmented Lagrangian and minimizing the

linearized augmented Lagrangian w.r.t. each variable. Let us denote the dual variable for the equality constraint by  $U_x$  and abuse notation to show the indicator function over each element of matrix  $W$  by  $\iota_{[0,1]}(W)$  where  $\iota_\Omega(x)$  takes the value 0 if  $x \in \Omega$ , otherwise infinity. The augmented Lagrangian can be written as in (4).

$$\begin{aligned} \mathcal{L}(L, W, U_x) &= \|L\|_* + \lambda_w \|W\|_1 + \iota_{[0,1]}(W) \\ &\quad + \langle U_x, (1 - W) \circ (L - X) \rangle \\ &\quad + \frac{\rho_x}{2} \|(1 - W) \circ L - (1 - W) \circ X\|^2 \end{aligned} \quad (4)$$

**Definition 2.1.** For simplicity, let us define the following notation, where superscript  $i$  denotes the iteration number.

$$\Lambda_L^i \triangleq (1 - W^i) \circ \left( (L^i - X) \circ (1 - W^i) + \frac{U_x^i}{\rho_x} \right)$$

$$\Lambda_W^i \triangleq (X - L^{i+1}) \circ \left( (L^{i+1} - X) \circ (1 - W^i) + \frac{U_x^i}{\rho_x} \right)$$

**Definition 2.2.** Given matrix  $Y \in \mathbb{R}^{m \times n}$  and  $\delta > 0$ , let  $Y = U\Sigma V^T$  and  $I$  the identity matrix then,  $\mathcal{D}(Y, \delta) = U(\Sigma - \delta I)_+ V^T$  where  $(a)_+ = \max\{0, a\}$  denotes the singular value thresholding operator.

**Definition 2.3.**  $\Pi_{[0,1]}$  denotes The projection onto the interval  $[0, 1]$ .

The update for  $L$  at each iteration is achieved by minimizing the linearized augmented Lagrangian while fixing the variables  $W^i$  and  $U_x^i$ :

$$L^{i+1} = \arg \min_L \|L\|_* + \frac{\rho_x}{2} \left\| (1 - W^i) \circ (L - X) + \frac{U_x^i}{\rho_x} \right\|^2$$

We can linearize the quadratic term as

$$\begin{aligned} \frac{1}{2} \left\| (1 - W^i) \circ (L - X) + \frac{U_x^i}{\rho_x} \right\|^2 &\simeq \frac{1}{2\tau_L} \|L - L^i\|^2 \\ &\quad + \langle \Lambda_L^i, L - L^i \rangle + \frac{1}{2} \left\| (L^i - X) \circ (1 - W^i) + \frac{U_x^i}{\rho_x} \right\|^2 \end{aligned}$$

where  $\tau_L > 0$  is the proximal parameter. As a result the update rule for  $L$  can be written as in (5).

$$\begin{aligned} L^{i+1} &= \arg \min_L \|L\|_* + \frac{\rho_x}{2\tau_L} \|L - (L^i - \tau_L \Lambda_L^i)\|^2 \\ &= \mathcal{D} \left( L^i - \tau_L \Lambda_L^i, \frac{\tau_L}{\rho_x} \right) \end{aligned} \quad (5)$$

The update rule for  $W$  is achieved by minimizing the linearized augmented Lagrangian while fixing  $L^{i+1}$  and  $U_x^i$ . Using the same technique we have

$$\begin{aligned} \frac{1}{2} \left\| (1 - W) \circ (L^{i+1} - X) + \frac{U_x^i}{\rho_x} \right\|^2 &\simeq \frac{1}{2\tau_W} \|W - W^i\|^2 \\ &\quad + \langle \Lambda_W^i, W - W^i \rangle + \frac{1}{2} \left\| (L^{i+1} - X) \circ (1 - W^i) + \frac{U_x^i}{\rho_x} \right\|^2 \end{aligned}$$

where  $\tau_W \geq 0$  is the proximal parameter. As a result, the update rule for  $W$  can be written as

$$\begin{aligned} W^{i+1} &= \arg \min_W \lambda_w \|W\|_1 + \iota_{[0,1]}(W) \\ &\quad + \frac{\rho_x}{2\tau_W} \|W - (W^i - \tau_W \Lambda_W^i)\|^2 \\ &= \Pi_{[0,1]} \left[ \text{soft} \left( W^i - \tau_W \Lambda_W^i, \frac{\lambda_w \tau_W}{\rho_x} \right) \right] \end{aligned} \quad (6)$$

The update rule for  $U_x$  is done by dual ascent as

$$U_x^{i+1} = U_x^i + \rho_x \left( (1 - W^{i+1}) \circ (L^{i+1} - X) \right) \quad (7)$$

The steps of the algorithm are summarized in Alg. 1.

**Alg. 1:** ADMM with linearizing applied to Eq. (3)

---

```

1 Input:  $X, \lambda_w, \rho_x$ ;
2  $L \leftarrow \text{median}(X)$   $W \leftarrow 0$   $U_x \leftarrow 0$ ;
3 while not converged do
    //Main operations detailed in comments
    //Singular Value Thresholding (5)
4  $L \leftarrow \arg \min_{\mathbf{A}} \hat{\mathcal{L}}_L(\mathbf{A}, W, U_x)$ 
    //Soft-thresholding & projection (6)
5  $W \leftarrow \arg \min_{\mathbf{A}} \hat{\mathcal{L}}_W(L, \mathbf{A}, U_x)$ 
    //Element-wise mult and add (7)
6  $U_x \leftarrow U_x + \rho_x \left( (1 - W) \circ (X - L) \right)$ ;
7 Output:  $L, W$ ;
    
```

---

### 2.1.1. CONVERGENCE ANALYSIS

In this section, we state and prove results regarding the convergence analysis of the proposed algorithm for solving (3).

**Proposition 1.** Linear independence constraint qualification (LICQ) holds for the problem in (3).

**Proposition 2.** Denote the variable at next iteration by superscript  $+$  then, the update of the dual variable  $U_x$  increases the augmented Lagrangian such that

$$\mathcal{L}(L^+, W^+, U_x^+) - \mathcal{L}(L^+, W^+, U_x) = \frac{1}{\rho_x} \|U_x^+ - U_x\|$$

*Proof.* This can be proved using the augmented Lagrangian in (4) and the update rule for  $U_x$ . The proof is provided in the supplementary material.  $\square$

**Proposition 3.** Suppose that  $\|U_x^{i+1} - U_x^i\| \rightarrow 0$ . Then,  $\nabla_{U_x} \mathcal{L}(L, W, U_x) \rightarrow 0$  and every limit point of the sequence  $\{(L^i, W^i)\}_0^\infty$  is feasible.

*Proof.* The proof is provided in the supplementary material.  $\square$

**Proposition 4.** Let  $\partial f(x)$  denote the general subdifferential of  $f$  at  $x$  (Rockafellar & Wets, 2009), then

$$-\frac{\rho_x}{\tau_L} (L^{i+1} - L^i) - \rho_x \Lambda_L^i \in \partial f(L^{i+1}) \quad (8)$$

$$-\frac{\rho_x}{\tau_W} (W^{i+1} - W^i) - \rho_x \Lambda_W^i \in \partial g(W^{i+1}) \quad (9)$$

where  $f(L) = \|L\|_*$  and  $g(W) = \lambda_w \|W\|_{1+\iota_{[0,1]}}(W)$ .

*Proof.* The two statements can be checked from the optimality conditions of (5) and (6).  $\square$

**Proposition 5.** Assume the sequence  $\{(L^i, W^i, U_x^i)\}_0^\infty$  is bounded, then every limit point  $(L^\infty, W^\infty, U_x^\infty)$  is a Karush–Kuhn–Tucker (KKT) point of (3).

*Proof.*  $\{(L^i, W^i, U_x^i)\}_0^\infty$  is bounded, hence from Proposition 3 every limit point  $(L^\infty, W^\infty)$  satisfies  $(1 - W^\infty) \circ (L^\infty - X) = 0$ . Additionally, by Proposition 4 and the definition of the general sub-gradient (Rockafellar & Wets, 2009), we get  $f(L) \geq f(L^i) + \langle L - L^i, -\frac{\rho_x}{\tau_L} (L^i - L^{i-1}) - \rho_x \Lambda_L^{i-1} \rangle \forall L$ . Letting  $i \rightarrow \infty$  and using the limit point feasibility we get  $f(L) \geq f(L^\infty) + \langle L - L^\infty, -(1 - W^\infty) \circ U_x^\infty \rangle \forall L$  resulting in  $-(1 - W^\infty) \circ U_x^\infty \in \partial f(L^\infty)$ . Similarly, we can show that  $-(L^\infty - X) \circ U_x^\infty \in \partial g(W^\infty)$ , hence concluding the KKT condition for the limit points.  $\square$

### 3. Extension of M-RPCA

In this section, we further extend the proposed formulation to handle more challenging scenarios such as cases where changes in the background are present. Our goal is to consider more realistic and challenging scenarios, that dynamic background is present and extend the framework to tackle such cases. Additionally, we enforce spacial and temporal connectivity of the foreground mask.

Let us consider a case where dynamic changes are present as part of the background (such as the motion of leaves in the wind). In the original RPCA such changes would be considered as dynamic perturbations to the static background and will be separated to the sparse component which in turn would result in the noise appearing on the mask after thresholding the sparse component.

The formulation in (3) is prone to a similar problem as the RPCA. Let us consider the presence of dynamic changes in the background and the equality constraint in (3). Depending on the value of  $\lambda_w$  in (3), the contribution of these small changes is either considered as part of the foreground mask or will stay present on the estimated background. To further explain, consider large value of  $\lambda_w$  and severe random noise as the perturbation. In such case, the cost of adding extra pixels to the mask is high and since the equality constraint

has to be satisfied, it would be plausible to accept the noise term on the  $L$  variable (which results in a slightly higher value for the nuclear norm) to satisfy the constraint. On the other hand, for small values of  $\lambda_w$  the noise will be picked by the foreground mask (satisfying the constraint) which is not appealing.

In order to extend the formulation such that it can handle dynamic background and is robust to noise, we can slightly change the equality constraint and use more regularization terms. Our prior knowledge about the foreground mask is that it contains more or less connected components as opposed to the dynamic background which has a more random and sparse nature. As a result, we can change the equality constraint to be  $(1 - W) \circ (X - L) = E$  where  $E$  is assumed to be the sparse perturbation. In this case,  $L$  does not have to match  $X$  where ever  $W$  is nonzero and the difference will be considered as part of  $E$ . We further need to enforce our prior knowledge (sparsity of  $E$  and spacial connectivity of  $W$ ) as regularization terms in the objective function. Let us first define some notation.

**Definition 3.1.** For a 3D matrix  $T \in \mathbb{R}^{m \times n \times k}$  let

$$\|DT\|_1 \triangleq \left\| \left( (D_h T)_{ijk}^2 + (D_v T)_{ijk}^2 + (D_d T)_{ijk}^2 \right)^{1/2} \right\|_1$$

with  $D_h, D_v, D_d$  being the horizontal, vertical, and depth derivative operators, respectively, then  $\|DT\|_1$  denotes the total variation (TV-norm) of the matrix  $T$  (Ng et al., 2010).

**Definition 3.2.** For a 3D matrix  $T \in \mathbb{R}^{m \times n \times k}$  let  $\mathcal{R}(T) \triangleq [\text{vec}(T_{\cdot 1}), \dots, \text{vec}(T_{\cdot k})]$  denote the reshape operator from a 3D matrix to a 2D matrix by stacking the frames as columns and the  $\mathcal{R}^{-1}(\cdot)$  as the inverse operator.

In order to enforce spatial connectivity of the foreground mask, we can regularize the total variation (TV-norm) of estimated foreground mask. Noting that the TV-norm only regularizes the changes, we would also like to regularize the total energy of the mask such that ideally the estimated mask would be piece-wise constant with most values set to zero. In order to enforce that, we add the sparsity of the noise contribution through  $\ell_1$ -norm. As a result, the problem can be formulated as in (3).

$$\begin{aligned} & \underset{L, W, E}{\text{minimize}} && \|L\|_* + \underbrace{\lambda_e \|E\|_1}_{\text{sparse noise}} \\ & && + \underbrace{\lambda_w \|W\|^2 + \lambda_z \|\mathcal{DR}^{-1}(W)\|_1}_{\text{enforce connectivity of the foreground}} \\ & \text{subject to:} && (1 - W) \circ (X - L) = E, \quad W \in [0, 1]^{mn \times k} \end{aligned}$$

Adding another extra variable  $Z$  to this formulation makes the solution via ADMM with linearizing techniques possi-

ble.

$$\begin{aligned}
 & \underset{L, W, Z, E}{\text{minimize}} && \|L\|_* + \lambda_w \|W\|^2 + \lambda_z \|Z\|_1 + \lambda_e \|E\|_1 \\
 & \text{subject to:} && (1 - W) \circ (X - L) = E \\
 & && D_{3D}(W) = Z, \quad W \in [0, 1]^{mn \times k}
 \end{aligned} \tag{10}$$

where  $D_{3D}(\cdot) = D\mathcal{R}^{-1}(\cdot)$ .

In the following part we derive the algorithm for solving (10) using the ADMM approach with linearizing with respect to the coupled variables. First, we form the augmented Lagrangian by introducing the dual variables  $U_x$  and  $U_z$  for the equality constraints as in (11). Then, we minimize the augmented Lagrangian w.r.t. each variable while keeping the others fixed and linearizing the quadratic term with the coupled variables.

$$\begin{aligned}
 \mathcal{L}(L, W, Z, E, U_x, U_z) &= \|L\|_* + \lambda_z \|Z\|_1 + \lambda_e \|E\|_1 \\
 &+ \lambda_w \|W\|^2 + \iota_{[0,1]}(W) + \langle U_z, Z - D_{3D}(W) \rangle \\
 &+ \frac{\rho_z}{2} \|Z - D_{3D}(W)\|^2 + \langle U_x, (1 - W) \circ (L - X) + E \rangle \\
 &+ \frac{\rho_x}{2} \|(1 - W) \circ (L - X) + E\|^2
 \end{aligned} \tag{11}$$

**Definition 3.3.** for simplicity of the notation let us define  $\Psi_L^i \triangleq (1 - W^i) \circ \left( (L^i - X) \circ (1 - W^i) + E^i + \frac{U_x^i}{\rho_x} \right)$  and  $\Psi_W^i \triangleq (X - L^{i+1}) \circ \left[ (L^{i+1} - X) \circ (1 - W^i) + E^i + \frac{U_x^i}{\rho_x} \right]$  and  $\hat{\Psi}_W^i \triangleq W^i - \tau_W \Psi_W^i$ .

The update rule for  $L$  has the same form as the previous section so it can be linearized by following similar steps and we get,

$$\begin{aligned}
 L^{i+1} &= \arg \min_L \|L\|_* + \frac{\rho_x}{2\tau_L} \|L - (L^i - \tau_L \Psi_L^i)\|^2 \\
 &= \mathcal{D} \left( L^i - \tau_L \Psi_L^i, \frac{\tau_L}{\rho_x} \right)
 \end{aligned} \tag{12}$$

The update rule for  $W$  can be written as

$$\begin{aligned}
 W^{i+1} &= \arg \min_W \lambda_w \|W\|^2 + \iota_{[0,1]}(W) \\
 &+ \frac{\rho_z}{2} \left\| Z^i - D_{3D}(W) + \frac{U_z^i}{\rho_z} \right\|^2 \\
 &+ \frac{\rho_x}{2} \left\| (1 - W) \circ (L^{i+1} - X) + E^i + \frac{U_x^i}{\rho_x} \right\|^2
 \end{aligned} \tag{13}$$

and by linearizing the last term in the right hand side of (13) we get the following minimization problem.

$$\begin{aligned}
 W^{i+1} &= \arg \min_W \lambda_w \|W\|^2 + \iota_{[0,1]}(W) \\
 &+ \frac{\rho_z}{2} \left\| Z^i - D_{3D}(W) + \frac{U_z^i}{\rho_z} \right\|^2 + \frac{\rho_x}{2} \|W - \Psi_W^i\|^2
 \end{aligned} \tag{14}$$

The computationally efficient solution can be achieved by employing the Fourier transform and solving a diagonal system of equations (element-wise division).

$$W^{i+1} = \Pi_{[0,1]} \left[ \mathcal{R}\mathcal{F}^{-1} \frac{\mathcal{F}(\mathcal{R}^{-1}(\Gamma))}{(\alpha I + \rho_z \Sigma_D^H \Sigma_D)} \right] \tag{15}$$

where  $\alpha = 2\lambda_w + \rho_x/\tau_W$ ,  $\mathcal{F}$  and  $\mathcal{F}^{-1}$  are the 3D Fourier transform pair,  $\Sigma_D = \mathcal{F}^{-1} D \mathcal{F}$ , and  $\Gamma = \frac{\rho_x}{\tau_W} \hat{\Psi}_W^i + \rho_z \mathcal{R}(D^T(Z + U_z/\rho_z))$ .

The update rule for  $E$  is achieved by minimizing the augmented Lagrangian w.r.t.  $E$  which results in element-wise soft-thresholding as

$$\begin{aligned}
 E^{i+1} &= \arg \min_E \lambda_e \|E\|_1 \\
 &+ \frac{\rho_x}{2} \left\| E + (1 - W^{i+1}) \circ (L^{i+1} - X) + \frac{U_x^i}{\rho_x} \right\|^2 \\
 &= \text{soft} \left( (W^{i+1} - 1) \circ (L^{i+1} - X) - \frac{U_x^i}{\rho_x}, \frac{\lambda_e}{\rho_x} \right)
 \end{aligned} \tag{16}$$

The update rule for  $Z$  is achieved by solving the minimization problem as in (17) where the proximal operator is denoted by  $\text{shrink}(\cdot)$  (Ng et al., 2010).

$$\begin{aligned}
 Z^{i+1} &= \arg \min_Z \lambda_z \|Z\|_1 + \frac{\rho_z}{2} \left\| Z - D_{3D}(W^i) + \frac{U_z^i}{\rho_z} \right\|^2 \\
 &= \text{shrink} \left( D_{3D}(W^{i+1}) - \frac{U_z^i}{\rho_z}, \frac{\lambda_z}{\rho_z} \right)
 \end{aligned} \tag{17}$$

The dual variables are updated according to the equality constraints as in (18) and (19).

$$U_x^{i+1} = U_x^i + \rho_x \left( (1 - W^{i+1}) \circ (L^{i+1} - X) + E^{i+1} \right) \tag{18}$$

$$U_z^{i+1} = U_z^i + \rho_z (Z^{i+1} - D_{3D}(W^{i+1})) \tag{19}$$

### 3.1. Computational Complexity

In this part, we briefly discuss the computational complexity of the proposed algorithms. The most computationally demanding step of the Algorithm 1 is the singular value thresholding step which is the same as the original RPCA via principal component pursuit. In recent years, variety of different methods have been developed to reduce the computation cost of the PCP algorithm. For instance, the computation of the SVD can be reduced using the power method (Pope et al., 2011). We would like to note that all these methods are also applicable to the proposed algorithms in this study. For Algorithm 2, in addition to the singular value thresholding computation of the Fourier transform is also required which can be done in  $\mathcal{O}(mn \log(mn))$  time using the Fast Fourier Transform.

**Alg. 2:** ADMM with linearizing applied to Eq. (10)

---

```

1 Input:  $X, \lambda_w, \lambda_z, \lambda_s, \rho_x, \rho_z;$ 
2  $L \leftarrow \text{median}(X)$   $W \leftarrow 0$   $Z \leftarrow 0$   $E \leftarrow 0$ 
    $U_x \leftarrow 0$   $U_z \leftarrow 0;$ 
3 while not converged do
   //Singular Value Thresholding (12)
4  $L \leftarrow \arg \min_{\mathbf{A}} \widehat{\mathcal{L}}_L(\mathbf{A}, W, Z, E, U_x, U_z)$ 
   //FFT & diag solve & iFFT (15)
5  $W \leftarrow \arg \min_{\mathbf{A}} \widehat{\mathcal{L}}_W(L, \mathbf{A}, Z, E, U_x, U_z)$ 
   //Element-wise clipping (17)
6  $Z \leftarrow \arg \min_{\mathbf{A}} \mathcal{L}(L, W, \mathbf{A}, E, U_x, U_z)$ 
   //Soft-thresholding (16)
7  $E \leftarrow \arg \min_{\mathbf{A}} \mathcal{L}(L, W, Z, \mathbf{A}, U_x, U_z)$ 
   //Element-wise mult and add (18)
8  $U_x \leftarrow U_x + \rho_x ((1 - W) \circ (L - X) + E);$ 
   //Element-wise add and subtract (19)
9  $U_z \leftarrow U_z + \rho_z (Z - D_{3D}(W));$ 
10 Output:  $L, W, E;$ 

```

---

## 4. Experimental Results and Discussion

In this section, we present several experiments and comparisons on real-world video sequences with a variety of scenarios. For the experiments with static background we use the Baseline category from the Change Detection (CDnet) dataset (Wang et al., 2014) and for the dynamic background case we use the I2R dataset (Li et al., 2004). In our evaluations we shall use both statistical measures and visual comparisons. Considering the number of true positive (tp), true negative (tn), false positive (fp), and false negative (fn), the recall ( $\text{Re} = \text{tp}/(\text{tp}+\text{fn})$ ), Precision ( $\text{Pre} = \text{tp}/(\text{tp}+\text{fp})$ ), and F-measure ( $\text{F1} = 2 \frac{\text{Pre} \times \text{Re}}{\text{Pre} + \text{Re}}$ ) are employed as quantitative metrics to evaluate the performance of the foreground detection.

### 4.1. Results for Static Background

In our first experiment we consider the video sequences with static background and investigate different settings for the M-RPCA as in (3), EM-RPCA as in (10), and RPCA. Here, we use 100 frames from different challenging parts of the Baseline videos in CDnet. The qualitative and quantitative results are presented in Fig. 2 and Table 1 respectively. As we can observe, increase in  $\lambda_w$  for M-RPCA results in increase in precision and decrease in recall (similar trade-off is present for RPCA w.r.t. the threshold value). M-RPCA shows improvement over RPCA in general while keeping the recall and precision at relatively high levels.

As we can see from the results of EM-RPCA in Table 1, considering the spacial connectivity increases the performance in the presence of multiple and overlapping objects. For the

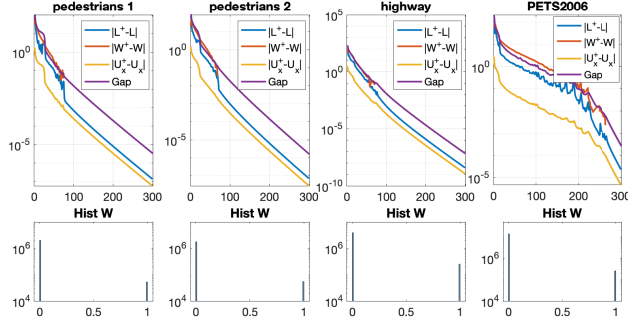


Figure 1. Empirical convergence results of the Algorithm 1 for four different datasets.

PETS2006, since the man in the back is fairly stationary in the entire sequence, enforcing the connectivity results in more zeros in the mask of that region.

The convergence properties of the Algorithm 1 for different datasets is shown in Fig. 1. We can observe that the variables have converged and the  $\|(1 - W) \circ (X - L)\|$  (denoted as Gap) converges to zero which shows the satisfaction of the assumptions in convergence analysis as well as feasibility of the final result. The histogram of the resulting  $W$  for M-RPCA, shown in the second row, illustrates the fact that in all the cases the binary mask is directly recovered.

We additionally compare the result of M-RPCA to other methods in the literature over other challenging sequences from CDnet. The experiments in this case closely follow the experimental setup in (Ye et al., 2015). As it can be seen from Table 2, the M-RPCA outperforms the other RPCA based methods. In the Winter sequence, due to the artifact present, M-RPCA is outperformed by DECOLOR (Zhou et al., 2013).

### 4.2. Results for the Extended M-RPCA and Dynamic Background

In this section we will show experimental results using the EM-RPCA as in (10) with dynamic background videos. First, we show the robustness of EM-RPCA to random noise, by adding synthetic noise to stationary background sequence and evaluate the performance of different methods. The results of our model compared with RPCA are shown in Table 3 and Fig. 3. As it can be seen EM-RPCA achieves good performance in terms of peak signal-to-noise ratio (PSNR) of the recovered background and the F-measure of the recovered mask.

In order to evaluate the performance of the EM-RPCA, dynamic background sequences from CDnet and I2R dataset are used. As an example, Figure 5 shows the low-rank, foreground mask and dynamic background components recovered by EM-RPCA. We compare our results to the RPCA and TVRPCA (Cao et al., 2016). TVRPCA generalizes RPCA for the dynamic background cases by decomposing

## Masked Robust Principal Component Analysis



Figure 2. Effect of parameters. columns l to r: original frame, ground truth, moderate, high, and low values of  $\lambda_w$  in M-RPCA, low to high threshold for RPCA, and RPCA thresholded with Otsu method. Rows t to b: Pedestrian1, Pedestrian2, Highway, and PETS2006

Table 1. Quantitative comparison of M-RPCA (3), EM-RPCA (10), and RPCA. for static background. The parameter for M-RPCA  $\{\lambda_w\}$ , RPCA (threshold value to obtain the mask), and EM-RPCA  $\{\lambda_w, \lambda_z, \lambda_e\}$  are indicated in the "PARAM" columns

	PEDESTRIANS 1				PEDESTRIANS 2				HIGHWAY				PETS2006			
	PARAM	RE	PRE	F1	PARAM	RE	PRE	F1	PARAM	RE	PRE	F1	PARAM	RE	PRE	F1
M-RPCA	1E-3	0.97	0.97	<b>0.97</b>	7E-4	0.85	0.83	0.84	9E-4	0.7	0.94	0.80	5E-5	0.76	0.81	<b>0.79</b>
	1E-4	0.99	0.67	0.80	7E-5	0.93	0.46	0.62	9E-5	0.92	0.68	0.78	5E-6	0.84	0.70	0.76
	1E-2	0.4	1.00	0.49	7E-3	0.17	1.00	0.31	9E-3	0.03	0.97	0.05	5E-4	0.60	0.97	0.74
EM-RPCA	1E-5				1E-5				1E-5				1E-5			
	1E-5	0.94	0.96	0.95	1E-5	0.88	0.87	<b>0.88</b>	1E-5	0.94	0.89	<b>0.92</b>	1E-5	0.64	0.79	0.71
	5E-3				5E-3				5E-3				5E-3			
RPCA	0.45	0.84	1.00	0.91	0.45	0.59	0.99	0.74	0.35	0.51	0.98	0.67	0.35	0.54	0.98	0.70
	0.5	0.88	1.00	0.93	0.5	0.67	0.95	0.80	0.4	0.59	0.95	0.73	0.45	0.65	0.93	0.76
	0.55	0.97	0.69	0.81	0.55	0.80	0.32	0.46	0.45	0.66	0.63	0.64	0.55	0.80	0.55	0.65
	OTSU	0.87	1.00	0.93	OTSU	0.58	0.99	0.73	OTSU	0.49	0.98	0.66	OTSU	0.60	0.95	0.74

Table 2. Comparison of M-RPCA with other methods over challenging videos from CDnet.

	SHADE			OFFICE			WINTER		
	RE	PRE	F1	RE	PRE	F1	RE	PRE	F1
<b>M-RPCA</b>	<b>0.77</b>	<b>0.80</b>	<b>0.79</b>	0.68	<b>0.83</b>	<b>0.74</b>	0.59	0.43	0.50
<b>DECOLOR</b> (ZHOU ET AL., 2013)	0.73	0.32	0.42	<b>0.87</b>	0.61	0.71	<b>0.64</b>	<b>0.70</b>	<b>0.69</b>
<b>GMM</b> (ZIVKOVIC, 2004)	0.75	0.71	0.72	0.53	0.82	0.59	0.39	0.58	0.45
<b>FBM</b> (ZHAO ET AL., 2012)	0.65	0.77	0.70	0.62	0.76	0.71	0.37	0.36	0.34
<b>RPCA</b> (CANDÈS ET AL., 2011)	0.69	0.74	0.71	0.57	0.76	0.62	0.55	0.40	0.42
<b>VIBE</b> (BARNICH & DROOGENBROECK, 2011)	0.74	0.78	0.76	0.7	0.8	0.69	0.57	0.18	0.23
<b>SOBS</b> (MADDALENA ET AL., 2008)	0.63	0.78	0.68	0.67	0.79	0.69	0.18	0.53	0.24

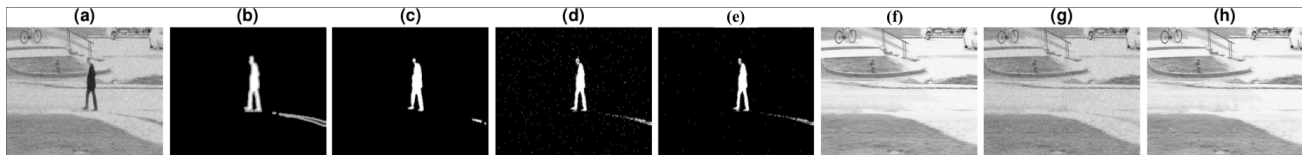


Figure 3. Visual results for synthetic noise. (a) noisy frame, (b) Ground truth, (c,f) EM-RPCA, (d,g) M-RPCA, and (e,h) RPCA.

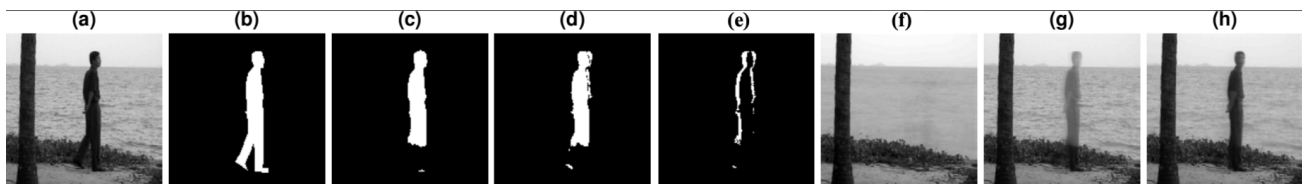


Figure 4. Visual results for WaterSurface: (a) original frame (b) Ground truth, mask from (c) EM-RPCA (d) TVRPCA (e) RPCA, low-rank image from (f) EM-RPCA (g) TVRPCA (h) RPCA.



Table 3. Comparison of different methods with synthetic noise

(SNR = 7.7dB)	PEDESTRIAN		HIGHWAY	
	F1	PSNR	F1	PSNR
EM-RPCA	0.94	34.65	0.90	30.80
M-RPCA	0.84	24.43	0.69	24.32
RPCA	0.90	34.10	0.60	31.14

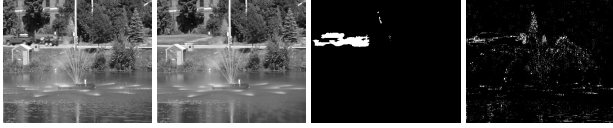


Figure 5. Different components by EM-RPCA form left to right: Original frame, low-rank component  $L$ , foreground mask  $W$ , and dynamic changes of background  $E$ .

the sparse component from the RPCA model into changing background and specially connected foreground. The EM-RPCA enforces the connectivity of the foreground based on the overlaying model. Table 4 shows the F-measures for different video sequences. TVRPCA and EM-RPCA perform similarly in terms of this measure.

Table 4. Comparison of EM-RPCA with different methods on dynamic background.

	EM-RPCA	TVRPCA	RPCA
WATERSURFACE	<b>0.88</b>	<b>0.88</b>	0.41
FOUNTAIN	<b>0.81</b>	0.80	0.57
CAMPUS	<b>0.77</b>	<b>0.77</b>	0.72
FOUNTAIN 2	0.71	<b>0.72</b>	0.43
OVERPASS	<b>0.78</b>	0.77	0.46

Visual results in Fig. 4 and Fig. 7 on the other hand show that overlaying model is better capable of recovering the background in case where the foreground stops moving. The ROC curve and the histogram of the  $W$  are shown in Fig. 6. The ROC curve shows slight improvement in terms of area under the curve. Additional visual results for another sequence are shown in Figures 8 and 9.

### 5. Conclusion

In this study, we introduced an extension of sparse and low-rank decomposition under overlaying model, and developed an optimization framework to solve it. We also propose an extension of our M-RPCA framework for the dynamic background. We also provide an analysis of the model convergence under reasonable assumptions. We performed an extensive experimental studies evaluating our model on multiple videos from CDnet and I2R datasets, and show improvements for both static and dynamic background over RPCA and its extensions. As future work, we plan to extend this framework for various scenarios such as camera jitter.

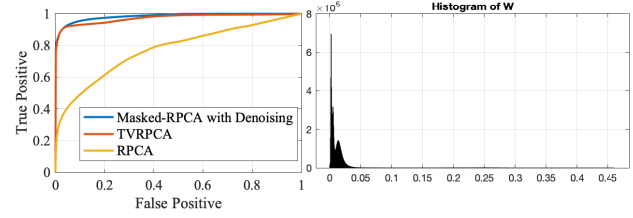


Figure 6. (left) ROC curve for the result of different methods on WaterSurface data. (right) Histogram of the recovered  $W$  from EM-RPCA.

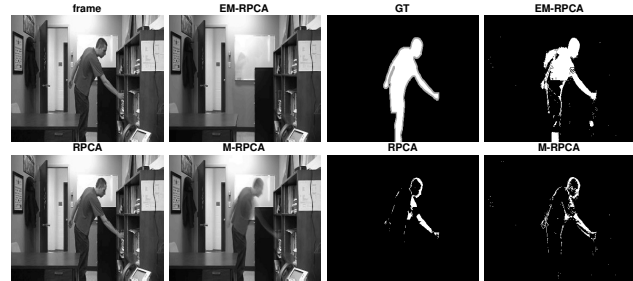


Figure 7. Visual results for the mask and the low-rank background for the slow moving sequence.

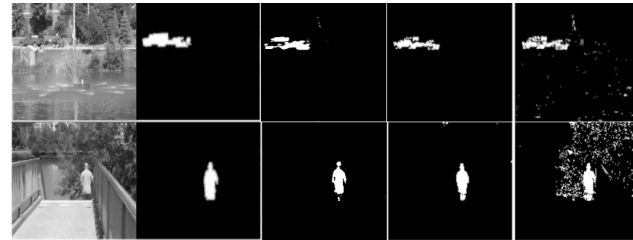


Figure 8. Visual results for the mask for Fountain2(top row) and Overpass(bottom row) datasets from CDnet. Images form left to right: Original frame, Ground truth mask, EM-RPCA mask, TVRPCA mask, and RPCA mask.



Figure 9. Visual results for the low-rank image for Fountain2(top row) and Overpass(bottom row) datasets from CDnet. Images form left to right: Original frame, low-rank component for EM-RPCA, and low-rank component for TVRPCA.



## References

- Barnich, O. and Droogenbroeck, M. V. Vibe: A universal background subtraction algorithm for video sequences. *IEEE Transactions on Image Processing*, 20(6):1709–1724, June 2011. ISSN 1057-7149. doi: 10.1109/TIP.2010.2101613.
- Boyd, S., Parikh, N., Chu, E., Peleato, B., Eckstein, J., et al. Distributed optimization and statistical learning via the alternating direction method of multipliers. *Foundations and Trends in Machine Learning*, 3(1):1–122, 2011.
- Candès, E. J., Li, X., Ma, Y., and Wright, J. Robust principal component analysis? *Journal of the ACM (JACM)*, 58(3):11, 2011.
- Cao, X., Yang, L., and Guo, X. Total variation regularized rpca for irregularly moving object detection under dynamic background. *IEEE Transactions on Cybernetics*, 46(4):1014–1027, April 2016. ISSN 2168-2267. doi: 10.1109/TCYB.2015.2419737.
- Chen, C.-F., Wei, C.-P., and Wang, Y.-C. F. Low-rank matrix recovery with structural incoherence for robust face recognition. In *Computer Vision and Pattern Recognition (CVPR), 2012 IEEE Conference on*, pp. 2618–2625. IEEE, 2012.
- Ebadi, S. E. and Izquierdo, E. Foreground segmentation via dynamic tree-structured sparse rpca. In *European Conference on Computer Vision*, pp. 314–329. Springer, 2016.
- Feng, J., Xu, H., and Yan, S. Online robust pca via stochastic optimization. In *Advances in Neural Information Processing Systems*, pp. 404–412, 2013.
- Gao, Z., Cheong, L.-F., and Wang, Y.-X. Block-sparse rpca for salient motion detection. *IEEE transactions on pattern analysis and machine intelligence*, 36(10):1975–1987, 2014.
- Goldfarb, D. Admm for multiaffine constrained optimization. 2018.
- Kafieh, R., Rabbani, H., and Selesnick, I. Three dimensional data-driven multi scale atomic representation of optical coherence tomography. *IEEE transactions on medical imaging*, 34(5):1042–1062, 2015.
- Keshavan, R. H., Montanari, A., and Oh, S. Matrix completion from noisy entries. *Journal of Machine Learning Research*, 11 (Jul):2057–2078, 2010.
- Li, L., Huang, W., Gu, I. Y.-H., and Tian, Q. Statistical modeling of complex backgrounds for foreground object detection. *IEEE Transactions on Image Processing*, 13(11):1459–1472, 2004.
- Lin, Z., Liu, R., and Su, Z. Linearized alternating direction method with adaptive penalty for low-rank representation. In Shawe-Taylor, J., Zemel, R. S., Bartlett, P. L., Pereira, F., and Weinberger, K. Q. (eds.), *Advances in Neural Information Processing Systems 24*, pp. 612–620. Curran Associates, Inc., 2011.
- Maddalena, L., Petrosino, A., et al. A self-organizing approach to background subtraction for visual surveillance applications. *IEEE Transactions on Image Processing*, 17(7):1168, 2008.
- Minaee, S. and Wang, Y. Masked signal decomposition using subspace representation and its applications. *arXiv preprint arXiv:1704.07711*, 2017.
- Ng, M. K., Weiss, P., and Yuan, X. Solving constrained total-variation image restoration and reconstruction problems via alternating direction methods. *SIAM journal on Scientific Computing*, 32(5):2710–2736, 2010.
- Peng, Y., Ganesh, A., Wright, J., Xu, W., and Ma, Y. Rasl: Robust alignment by sparse and low-rank decomposition for linearly correlated images. *IEEE Transactions on Pattern Analysis and Machine Intelligence*, 34(11):2233–2246, 2012.
- Pope, G., Baumann, M., Studer, C., and Durisi, G. Real-time principal component pursuit. In *Signals, Systems and Computers (ASILOMAR), 2011 Conference Record of the Forty Fifth Asilomar Conference on*, pp. 1433–1437. IEEE, 2011.
- Recht, B., Fazel, M., and Parrilo, P. A. Guaranteed minimum-rank solutions of linear matrix equations via nuclear norm minimization. *SIAM review*, 52(3):471–501, 2010.
- Rockafellar, R. T. and Wets, R. J.-B. *Variational analysis*, volume 317. Springer Science & Business Media, 2009.
- Wang, Y., Jodoin, P., Porikli, F., Konrad, J., Benzeeth, Y., and Ishwar, P. Cldnet 2014: An expanded change detection benchmark dataset. In *2014 IEEE Conference on Computer Vision and Pattern Recognition Workshops*, pp. 393–400, June 2014.
- Yang, J. and Yuan, X. Linearized augmented lagrangian and alternating direction methods for nuclear norm minimization. *Mathematics of computation*, 82(281):301–329, 2013.
- Yazdi, M. and Bouwmans, T. New trends on moving object detection in video images captured by a moving camera: A survey. *Computer Science Review*, 28:157–177, 2018.
- Ye, X., Yang, J., Sun, X., Li, K., Hou, C., and Wang, Y. Foreground-background separation from video clips via motion-assisted matrix restoration. *IEEE Transactions on Circuits and Systems for Video Technology*, 25(11):1721–1734, Nov 2015.
- Zhang, Y., Jiang, Z., and Davis, L. S. Learning structured low-rank representations for image classification. In *Proceedings of the IEEE Conference on Computer Vision and Pattern Recognition*, pp. 676–683, 2013.
- Zhang, Z., Ganesh, A., Liang, X., and Ma, Y. Tilt: Transform invariant low-rank textures. *International journal of computer vision*, 99(1):1–24, 2012.
- Zhao, Z., Bouwmans, T., Zhang, X., and Fang, Y. A fuzzy background modeling approach for motion detection in dynamic backgrounds. In *Multimedia and signal processing*, pp. 177–185. Springer, 2012.
- Zhou, X., Yang, C., and Yu, W. Moving object detection by detecting contiguous outliers in the low-rank representation. *IEEE Transactions on Pattern Analysis and Machine Intelligence*, 35 (3):597–610, March 2013.
- Zivkovic, Z. Improved adaptive gaussian mixture model for background subtraction. In *Pattern Recognition, 2004. ICPR 2004. Proceedings of the 17th International Conference on*, volume 2, pp. 28–31. IEEE, 2004.